Acta Biochim Biophys Sin 2026, 58(11): 2596–2608
https://cstr.cn/32197.14.abbs.2026041
https://doi.org/10.3724/abbs.2026041
Original Article

Original Article

Synergistic hepatic metabolic effects induced by coexposure to the fungicides carbendazim and procymidone in rats

Zhiwei Bao[1,2], Ting Luo[2], Shiyi Hu[1], Guiling Yang[2,3,*], and Yuanxiang Jin[1,*]

[1]College of Biotechnology and Bioengineering, Zhejiang University of Technology, Hangzhou 310032, China, [2]State Key Laboratory of Agricultural Products Safety/Key Laboratory of Detection for Pesticide Residues and Control of Zhejiang, Institute of Agro-product Safety and Nutrition, Zhejiang Academy of Agricultural Sciences, Hangzhou 310021, China, and [3]Biomanufacturing Research Institute of Xianghu Laboratory, Hangzhou 311231, China

*Correspondence address. E-mail: guilingchina2008@163.com (G.Y.); jinyx@zjut.edu.cn (Y.J.)

Received 17 October 2025 Accepted 22 January 2026 Published 26 May 2026

Abstract

Carbendazim (CBZ) and procymidone (PRO) are two fungicides widely used for decades. With excessive use, potential public health risks from their coresidues in vegetables and the environment have attracted increasing attention. Here, 6-week-old male SD rats are orally gavaged with 200 mg/kg CBZ, 200 mg/kg PRO, or 200 mg/kg CBZ + 200 mg/kg PRO (Mix group). At 1, 8 and 72 h postexposure, liver samples were collected and subjected to untargeted metabolomic analysis. Sparse partial least squares discriminant analysis (sPLS-DA) shows that all treatment groups exhibit significant separation from the Control group. Meanwhile, the Mix group is also significantly separated from the individual treatment groups. At 1 and 8 h postexposure, differentially abundant metabolites are predominantly enriched in fatty acyls according to HMDB classification, and the levels of 12-keto-eicosatetraenoic acid (12-KETE) are significantly elevated across treatment groups. 12-KETE acts as a PPARγ ligand and regulates PPARγ signaling pathways. The Mix-8 h group exhibits the largest number of differentially abundant metabolites. KEGG enrichment analysis identifies two uniquely enriched pathways with high impact (phenylalanine, tyrosine and tryptophan biosynthesis and linoleic acid metabolism). Within these pathways, linoleic acid, 13(S)-HPODE and L-tyrosine are significantly decreased only in the Mix-8 h group. Time-course analysis reveals diverse patterns of altered differentially abundant metabolites rather than a simple monotonic trend. Additionally, hepatic metabolite profiles remain separated among treatment groups after 72 h postexposure, although CBZ and PRO residues are hardly detected. Collectively, these results indicate that coexposure to CBZ and PRO amplifies hepatic metabolic disruption and produces mixture-specific toxic effects.

Key words carbendazim, procymidone, combined exposure, metabolomic

Introduction

Fungicides are important in agricultural production for controlling fungal diseases. Over the past decades, many different fungicides have been developed. Carbendazim (CBZ), a benzimidazole fungicide, binds to β-tubulin to inhibit fungal microtubule polymerization [1,2]. Procymidone (PRO), a dicarboximide fungicide, controls fungal growth by inhibiting spore germination, mycelial growth and triglyceride synthesis [3]. In agricultural production, these two fungicides have advantages such as broad-spectrum activity and cost-effectiveness [4,5]. Consequently, they have been widely used worldwide, including in China, Brazil and India, for decades [6,7]. The widespread application of CBZ and PRO has led to the frequent detection of their residues in fruits [8,9], vegetables [10] and Traditional Chinese Medicine [11]. In addition, Park *et al.* [12] reported that PRO was one of the most frequently detected fungicides in vegetables in South Korea. In Zhejiang, China, three years of surveillance revealed a high detection rate of PRO in tomato and eggplant [13]. Additionally, 82 pesticides were detected in the Jiulong River and estuary in South China, and all samples had PRO residuals [14]. Moreover, CBZ was detected in Brazil watercourse (maximum: 1396 ng/L) and Ebro Delta rice fields (maximum: 200 μg/L) [15,16].

Several previous studies have reported the individual toxic effects of CBZ and PRO on lipid metabolism [17], the inflammatory

© The Author(s) 2026. This is an open access article distributed under the terms of the Creative Commons Attribution License (https://creativecommons.org/licenses/by/4.0/).

response [18], development [19] and reproduction [20,21]. Our previous studies have demonstrated that CBZ exposure alters gut microbiota composition and induces liver lipid accumulation [18,22]. PRO acts as an anti-androgen by competitively inhibiting androgen binding to the androgen receptor [23]. In larval zebrafish, PRO exposure disrupted the expression of GABA-nervous genes and reduced swimming distance [24]. Recent evidences suggest that pesticide residues often consist of multiple compounds, and the potential impact of combined pesticide exposure on public health is receiving increased attention [11,25]. Wade *et al.* [26] reported that insecticide-fungicide combination exposure to larval honeybees caused lower survival to adulthood than the control or fungicide-only treatments. In addition, combined exposure to procymidone and chlorothalonil was reported to affect liver glycolipid metabolism and disrupt intestinal function [27]. Meanwhile, Di *et al.* [28] reported that the combined use of CBZ and PRO in strawberry greenhouses significantly increased dissipation half-lives compared with single use. However, studies on the potential toxic effects of combined exposure to CBZ and PRO remain limited, and further investigation is warranted.

Metabolomic analysis has been extensively used to explore the toxic effects of environmental pollutants on organisms [29,30]. For instance, Wang *et al.* [27] performed targeted metabolomic analysis and found that the combination of chlorothalonil and PRO affected serum acyl-carnitine profiles. Additionally, untargeted metabolomic analysis revealed the toxic effects of chlorothalonil, carbendazim and prochloraz in larval zebrafish and suggested that 2-aminoadipic acid might serve as a biomarker of exposure to these fungicide mixtures [31]. The liver serves as the primary organ for metabolism, detoxification and biotransformation of xenobiotics, making it the principal target for environmental pollutants [29,32]. Consistent with this, some previous studies have reported that individual exposure to either CBZ or PRO causes liver injury and metabolic disorders [17,22,33]. While the occurrence of CBZ and PRO in vegetables and the environment is well documented, the potential health risks of their mixture remain unclear.

In this study, we employed untargeted metabolomic analysis to elucidate hepatic toxicity induced by combined exposure to CBZ and PRO. Our findings provide new evidence for the combined toxic effects of CBZ and PRO on hepatic metabolic alterations, which will contribute to public health risk assessment and fungicide safety management.

Materials and Methods

Animals and experimental design

Male SD rats (5-week-old) were purchased from the China National Laboratory Animal Research Center (Shanghai, China), housed at four rats per cage, and raised at 22°C under a 12 h:12 h light-dark cycle. This work received approval for research ethics from the Institutional Research Ethics Committee of Zhejiang Academy of Agricultural Sciences. Two fungicides, carbendazim (CBZ, purity ≥ 97%) and procymidone (PRO, CAS No. 32809-16-8, purity ≥ 97%), obtained from Aladdin (Shanghai, China), were dissolved in corn oil.

After one week of acclimation, animals were randomly assigned to four groups: Control group (0 h, $n = 4$), CBZ group (200 mg/kg, $n = 12$), PRO group (200 mg/kg, $n = 12$) and Mix group (200 mg/kg CBZ + 200 mg/kg PRO, $n = 12$). Treatments were administered by oral gavage. Four control rats were euthanized at 0 h. For each treatment group, four rats were euthanized at 1, 8, and 72 h postgavage. Liver samples were rapidly excised, snap-frozen in liquid nitrogen and stored at −80°C for subsequent untargeted metabolomic analysis.

Hepatic untargeted metabolomics analysis

For the hepatic untargeted metabolomic analysis, liver tissues were extracted by adding 1 mL of extraction solvent consisting of 75% of a 9:1 methanol:chloroform mixture and 25% H_2O. Samples were homogenized twice at 50 Hz for 60 s, sonicated for 30 min at room temperature and incubated on ice for 30 min. Then, the extracts were centrifuged at 13,800 *g* for 10 min at 4°C, and the supernatants were transferred to fresh tubes. Extracts were reconstituted in 200 μL of 50% acetonitrile solution containing 2-amino-3-(2-chloro-phenyl)-propionic acid (4 ppm), vortexed and filtered through a 0.22-μm membrane for further LC-MS/MS detection. Chromatographic separation was performed on an ACQUITY UPLC HSS T3 column (150 mm × 2.1 mm, 1.8 μm) by an ACQUITY UPLC system (Waters, Milford, USA). The column temperature was held at 40°C. The mobile phase for positive model analysis was: (A) 0.1% (v/v) formic acid in acetonitrile and (B) 0.1% (v/v) formic acid in water and the gradient was (1) 0–1 min, 2% A, (2) 1–9 min, 2%–50% A, (3) 9–12 min, 50%–98% A, (4) 12–13.5 min, 98% A, (5) 13.5–14 min, 98%–2% A and (6) 14–20 min, 2% A. In addition, the mobile phase for negative model analysis was: (C) 0.1% (v/v) formic acid in acetonitrile and (D) 0.1% (v/v) formic acid in water, and the gradient was: (1) 0–1 min, 2% C, (2) 1–9 min, 2%–50% C, (3) 9–12 min, 50%–98% C, (4) 12–13.5 min, 98% C, (5) 13.5–14 min, 98%–2% C, and (6) 14–20 min, 2% C. Mass spectrometric analysis was performed on a Q Exactive Orbitrap mass spectrometer (Thermo Fisher Scientific, Waltham, USA) equipped with an electrospray ionization (ESI) source. Data were acquired in full MS/data-dependent MS/MS (Full MS-ddMS^2) mode. Source and acquisition parameters were as follows: sheath gas = 30 (arb. units); auxiliary gas = 10 (arb. units); spray voltage = +3.50 kV (ESI+) and −2.50 kV (ESI−); capillary temperature = 325°C. MS1 scans were acquired over m/z 81–1000 at 70,000 FWHM resolving power (at m/z 200), with up to 10 data-dependent MS/MS scans per cycle at 17,500 FWHM. Normalized collision energy (NCE) was set to 30%, and dynamic exclusion was enabled (automatic).

Hepatic differential abundant metabolites analysis

The KEGG pathway enrichment analysis of hepatic differentially abundant metabolites was performed by MetaboAnalyst [34]. The superclass and class of differentially abundant metabolites were enriched according to The Human Metabolomic Database (HMDB) [35]. The Venn diagram and Venn network diagram of differentially abundant metabolites were plotted in EVenn [36]. The time-course analysis of differentially abundant metabolites was performed by the R package Mfuzz [37].

Statistical analysis

The differentially abundant metabolites in the liver after exposure were filtered by $P < 0.05$ and $|\text{Log2Foldchange}| > 0.585$. Data are expressed as the mean ± SEM. The statistical significance was determined by *t*-test between the treated groups and the 0 h group via MetaboAnalyst [34]. $P < 0.05$ was considered to indicate statistically significant difference.

Results

Hepatic untargeted metabolomic analysis

The liver is the primary organ for energy metabolism and xenobiotic detoxification. To assess hepatic toxicity following binary exposure to CBZ and PRO, untargeted metabolomic analysis was performed to determine the hepatic metabolite profiles among the CBZ, PRO and Mix groups at 1, 8 and 72 h postexposure (Figure 1). The total ion chromatogram showed the hepatic metabolomic profiles (Figure 1A). In all 40 samples, sparse partial least squares discriminant analysis (sPLS-DA) was applied to visualize discrimination between treatment groups and the control group (0 h) (Figure 1B). The metabolites with the top 5 scores in loadings 1 and 2 are shown in

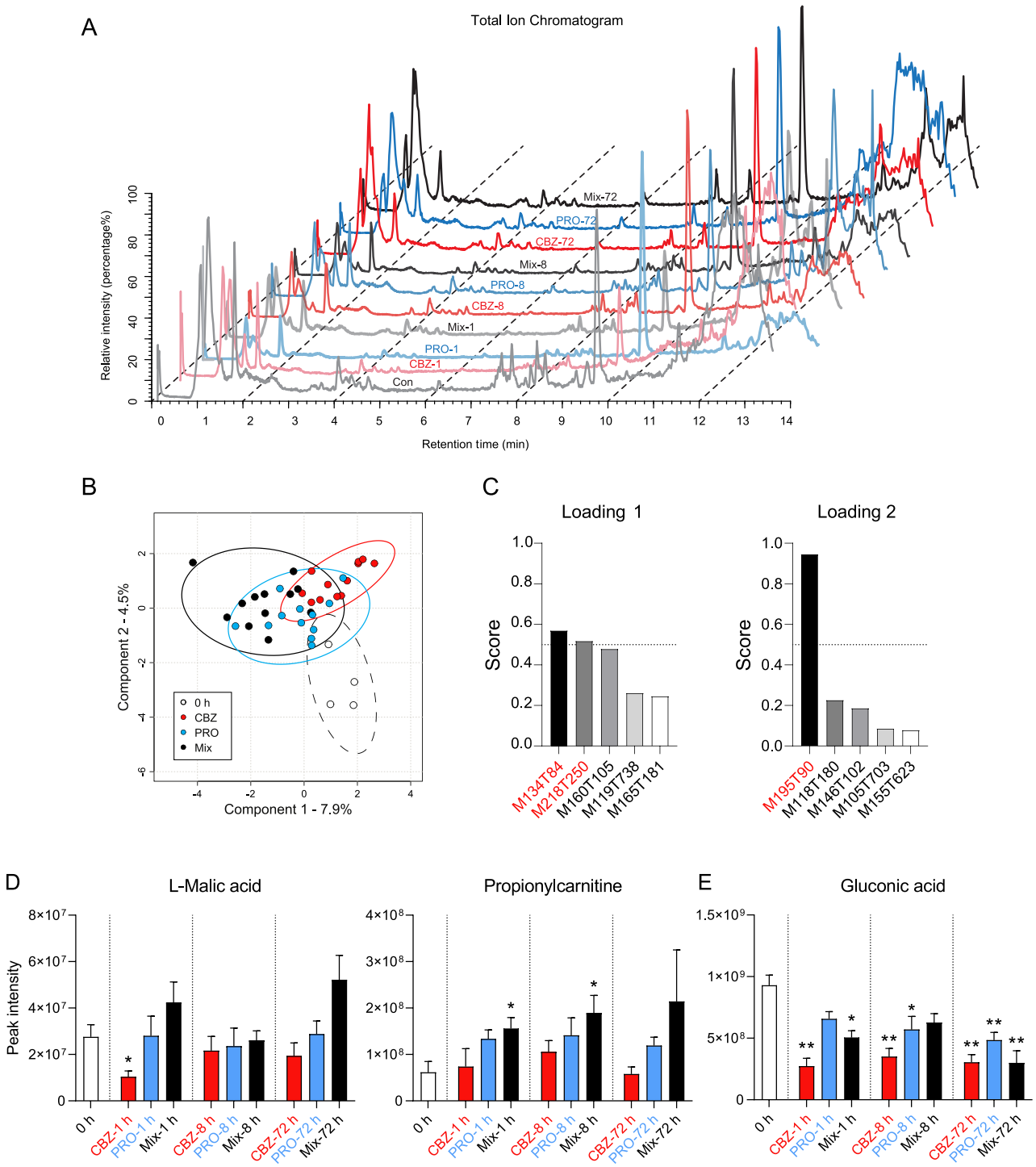


Figure 1. Hepatic untargeted metabolomic analysis after exposure to CBZ, PRO and Mix (A) The total ion chromatogram of hepatic untargeted metabolomics analysis by LC-MS/MS after exposure. (B) The sPLS-DA plot of all samples. (C) The top 5 scoring metabolites in loadings 1 and 2. (D) Two metabolites with loading score > 0.5 in loading 1, including L-malic (M134T84) and propionyl-carnitine (M218T250). (E) Gluconic acid (M195T90) with loading score > 0.5 in loading 2. Data are presented as the mean ± SEM (n = 4). *P < 0.05, **P < 0.01.

Figure 1C, and the metabolites with score > 0.5 in loadings 1 and 2 were L-malic acid (M134T84), propionylcarnitine (M218T250) and gluconic acid (M195T90) (Figure 1C). The contents of L-malic acid were significantly decreased in the CBZ-1 h group, and propionylcarnitine was significantly increased in the Mix-1 h and Mix-8 h groups (Figure 1D). In addition, the contents of gluconic acid were significantly decreased in the CBZ-1 h, Mix-1 h, CBZ-8 h, PRO-8 h, CBZ-72 h, PRO-72 h and Mix-72 h groups (Figure 1E).

The sPLS-DA results among CBZ, PRO and Mix groups at 1 or 8 h postexposure

Then, we compared the differences among CBZ, PRO and Mix treatments at 1 or 8 h postexposure (Figure 2). sPLS-DA was performed in the CBZ, PRO and Mix treatment groups after 1 or 8 h of exposure (Figure 2). At 1 h postexposure, the CBZ, PRO and Mix groups were significantly separated from the 0 h group, and the three treatment groups clustered closely (Figure 2A). The metabolites with the top 5 scores in loadings 1 and 2 were plotted (Figure 2B). Four metabolites had loading score > 0.5, including glucosamine (M160T105), fructose 1,6-bisphosphate (M339T78), gluconic acid (M195T90) and adenine (M134T277) (Figure 2B). The levels of glucosamine were significantly increased in the PRO-1 h and Mix-1 h groups, and fructose 1,6-bisphosphate was significantly increased in the PRO-1 h group (Figure 2C). The levels of gluconic acid and adenine were significantly decreased after CBZ, PRO and Mix treatment (Figure 2C). Additionally, the sPLS-DA results showed that the CBZ-8 h, PRO-8 h and Mix-8 h groups also had significant separation from the 0 h group (Figure 2D). Meanwhile, the Mix-8 h group was also significantly separated from the CBZ-8 h and PRO-8 h groups. Three metabolites had score > 0.5, including 16-hydroxy hexadecanoic acid (M271T829), pyrophosphate (M177T86) and hydroxyphenyllactic acid (M183T220) (Figure 2E). The levels of 16-hydroxy hexadecenoic acid and pyrophosphate were significantly decreased in the CBZ-8 h, PRO-8 h and Mix-8 h groups compared with those in the 0 h group (Figure 2F).

Differential hepatic metabolites after 1 and 8 h of administration

Then, the hepatic differentially abundant metabolites after 1 and 8 h of exposure were filtered by $P < 0.05$ and $|\mathrm{Log_2FoldChange}| > 0.585$ (Figure 3). The volcano plot showed the hepatic differentially abundant metabolites after CBZ, PRO and Mix treatment at 1 and 8 h postexposure (Supplementary Figure S1). After 1 h of exposure, 33, 45 and 32 hepatic differentially abundant metabolites were identified in the CBZ, PRO and Mix groups, respectively (Figure 3A and Supplementary Figure S1A–C). In addition, 44, 44 and 87 differentially abundant metabolites were observed after 8 h of exposure (Figure 3A and Supplementary Figure S1D–F). In the 1 h treatment groups, the PRO group had the largest number of differentially abundant metabolites compared with the CBZ-1 h and Mix-1 h groups (Figure 3A). At 8 h postexposure, the Mix-8 h group had the largest number of differentially abundant metabolites compared with the other two groups (Figure 3A). The Venn diagram and network detailed showed all hepatic differentially abundant metabolites in the CBZ, PRO and Mix treatment groups after 1 and 8 h of exposure (Figure 3B,C).

HMDB classification and KEGG pathway enrichment analysis of hepatic differentially abundant metabolites

Additionally, hepatic differentially abundant metabolites at 1 and 8 h postexposure were enriched according to the Human Metabolome Database (HMDB) in 30 Classes and 9 Superclasses (Figure 4). Aside from the Others class, hepatic differentially abundant metabolites were predominantly enriched in the top 3 Classes: (1) fatty acyls, (2) carboxylic acids and derivatives and (3) organooxygen compounds. Within the fatty acyls class, the Mix-8 h group had a greater number of differentially abundant metabolites than the individual CBZ and PRO treatment groups (Figure 4). Moreover, hepatic differentially abundant metabolites at 1 and 8 h postexposure were enriched by the KEGG database, including 43 level 2 pathways and 8 level 1 pathways (Figure 5). These enriched pathways from different treatment groups showed distinct patterns. For example, porphyrin metabolism, arginine biosynthesis, nitrogen metabolism and butanoate metabolism were enriched only in the CBZ-1 h and CBZ-8 h groups but not in the PRO or Mix treatment groups (Figure 5). Some pathways, such as amino sugar and nucleotide sugar metabolism, were enriched in both the PRO and Mix groups. In addition, biosynthesis of unsaturated fatty acids and arachidonic acid metabolism were enriched across the CBZ, PRO and Mix treatment groups. Consistent with Figure 3C, the peak intensity of 12-keto-eicosatetraenoic acid (12-KETE) was markedly increased after CBZ, PRO and Mix exposure at 1 and 8 h (Supplementary Figure S2A). We also observed that phenylalanine, tyrosine and tryptophan biosynthesis and linoleic acid metabolism were enriched with high impact only in the Mix-8 h group (Figure 5). In linoleic acid metabolism, the levels of linoleic acid 13-L-hydroperoxylinoleic acid [13(S)-HpODE] were significantly decreased in the Mix-8 h group compared with those in the 0 h group (Supplementary Figure S2B,C). For the phenylalanine, tyrosine and tryptophan biosynthesis pathways, the levels of L-tyrosine were significantly decreased in the Mix-8 h group compared with those the 0 h group (Supplementary Figure S2D).

sPLS-DA results of time-dependent changes after CBZ, PRO and Mix treatment

sPLS-DA analysis was performed to assess time-dependent changes after CBZ, PRO and Mix treatments (Figure 6). The sPLS-DA plot revealed a clear separation of the CBZ-exposed groups (1 and 8 h) from the 0 h group. The divergence between every treated and 0 h group increased as the time course progressed (Figure 6A). Similar results were also observed in the PRO and Mix treatment groups (Figure 6C,E). The hepatic differentially abundant metabolites in the CBZ-treated groups with loading score > 0.5 were gluconic acid (M195T90), 16-hydroxy hexadecanoic acid (M271T829) and L-glutamic acid (M148T96) (Figure 6B). The contents of gluconic acid and 16-hydroxy hexadecanoic acid were significantly decreased after CBZ treatment (Supplementary Figure S3A). The peak intensity of L-glutamic acid was significantly decreased in the CBZ-1 h group but significantly increased in the CBZ-8 h group (Supplementary Figure S3A). In addition, the differentially abundant metabolites of the PRO treatment groups with loading score > 0.5 were 16-hydroxy hexadecanoic acid (M271T829) and D-lyxose (M151T529) (Figure 6D). The levels of 16-hydroxy hexadecanoic acid were significantly decreased after PRO exposure, and the levels of D-lyxose were significantly increased in the PRO-8 h group (Supplementary Figure S3B). After mixed exposure, the differentially abundant metabolites with loading score > 0.5 were glucosamine (M160T105) and indolin-2-one (M134T449) (Figure 6F). The levels of glucosamine and indolin-2-one were both

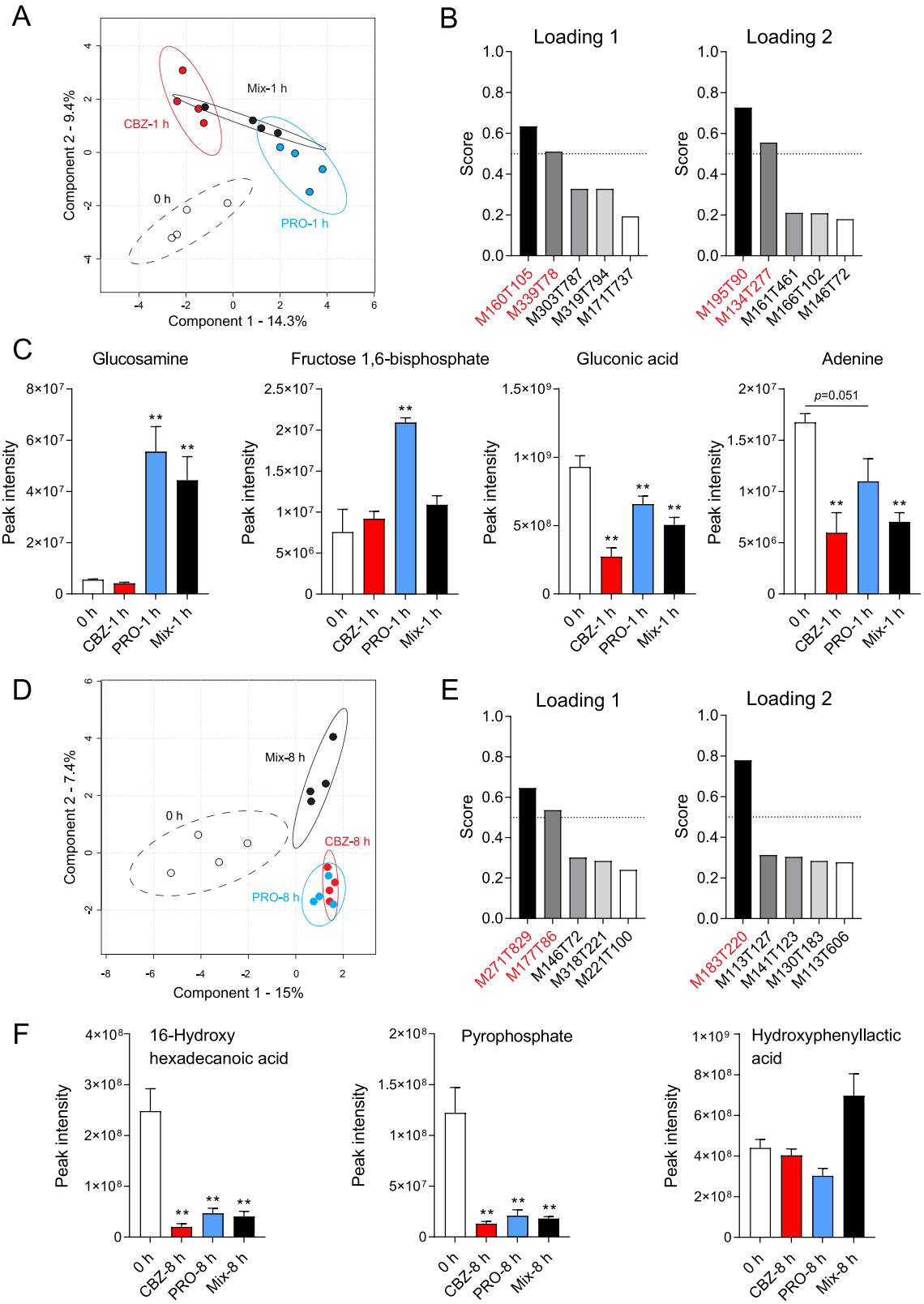


Figure 2. sPLS-DA results of different treatment groups (A) The sPLS-DA plot at 1 h postexposure with 0 h, CBZ-, PRO- and Mix-treated groups. (B) The loading scores for loadings 1 and 2 at 1 h postexposure. (C) The metabolites with loading score > 0.5 in loadings 1 and 2. (D) The sPLS-DA plot at 8 h postexposure with 0 h, CBZ-, PRO- and Mix-treated groups. (E) The loading scores for loadings 1 and 2 at 8 h postexposure. (F) The metabolites with loading score > 0.5 in loadings 1 and 2. Data are presented as the mean ± SEM (n = 4). $^{**}P < 0.01$.

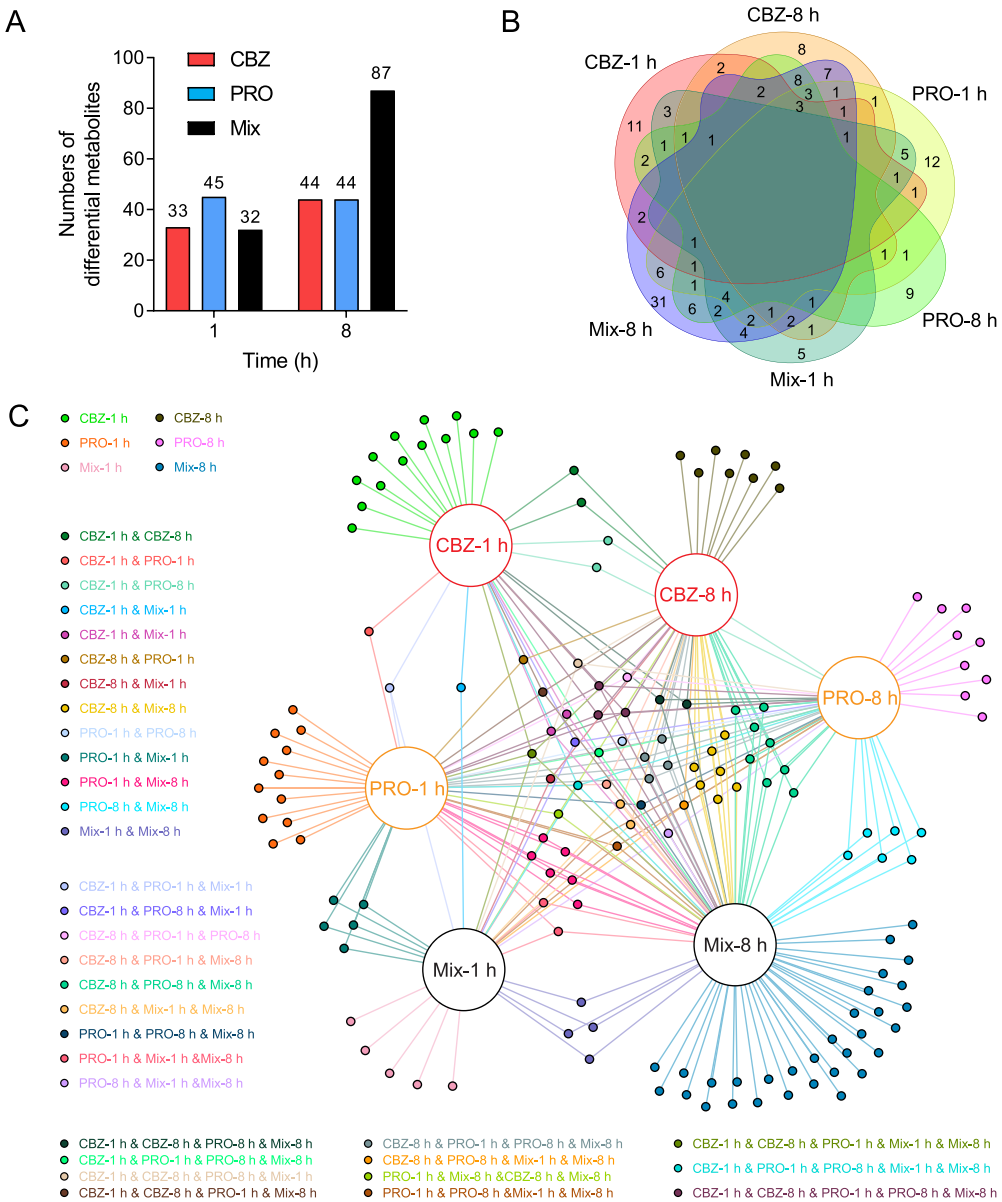


Figure 3. Hepatic differentially abundant metabolites after CBZ, PRO and Mix exposure (A) The number of hepatic differentially abundant metabolites after 1 and 8 h of exposure to CBZ, PRO and Mix. (B) Venn diagram of all differentially abundant metabolites in the six treatment groups. (C) Venn network diagram of all differentially abundant metabolites in the six treatment groups.

significantly increased in the Mix-1 h and Mix-8 h groups (Supplementary Figure S3C).

Time-course analysis of hepatic differentially abundant metabolites after 1 and 8 h of exposure

The above results indicated that CBZ, PRO and Mix exposure induced time-dependent changes in hepatic metabolite profiles. We therefore performed a time-course analysis to explore how differentially abundant metabolites changed after exposure. There was a total of 67, 75 and 104 hepatic differentially abundant metabolites after CBZ, PRO and Mix exposure, respectively (Figure 7). However, the number of common differentially abundant metabolites was only 10, 12 and 15 in the CBZ, PRO and Mix groups, respectively (Figure 7A,C,E). After CBZ, PRO and Mix exposure at 1 and 8 h postexposure, these differentially abundant metabolites were clustered by the R package Mfuzz. In each group, all differentially abundant metabolites were clustered into 6 clusters. In the CBZ treatment groups, most differentially abundant metabolites belonged to Clusters 2 (20.90%) and 4 (23.88%) (Figure 7B). For Cluster 4, these differentially abundant metabolites decreased sharply after 1 h of exposure and continued to decrease after 8 h of exposure (Figure 7B). After PRO exposure, most differentially abundant metabolites were clustered in Cluster 1 (21.05%) (Figure 7D). These differentially abundant metabolites showed an inverted-V shaped pattern (Figure 7D). After Mix exposure, most differentially abundant metabolites were clustered into Cluster 2 (23.08%) and Cluster 6 (21.15%) (Figure 7F). These differentially abundant metabolites showed continuously

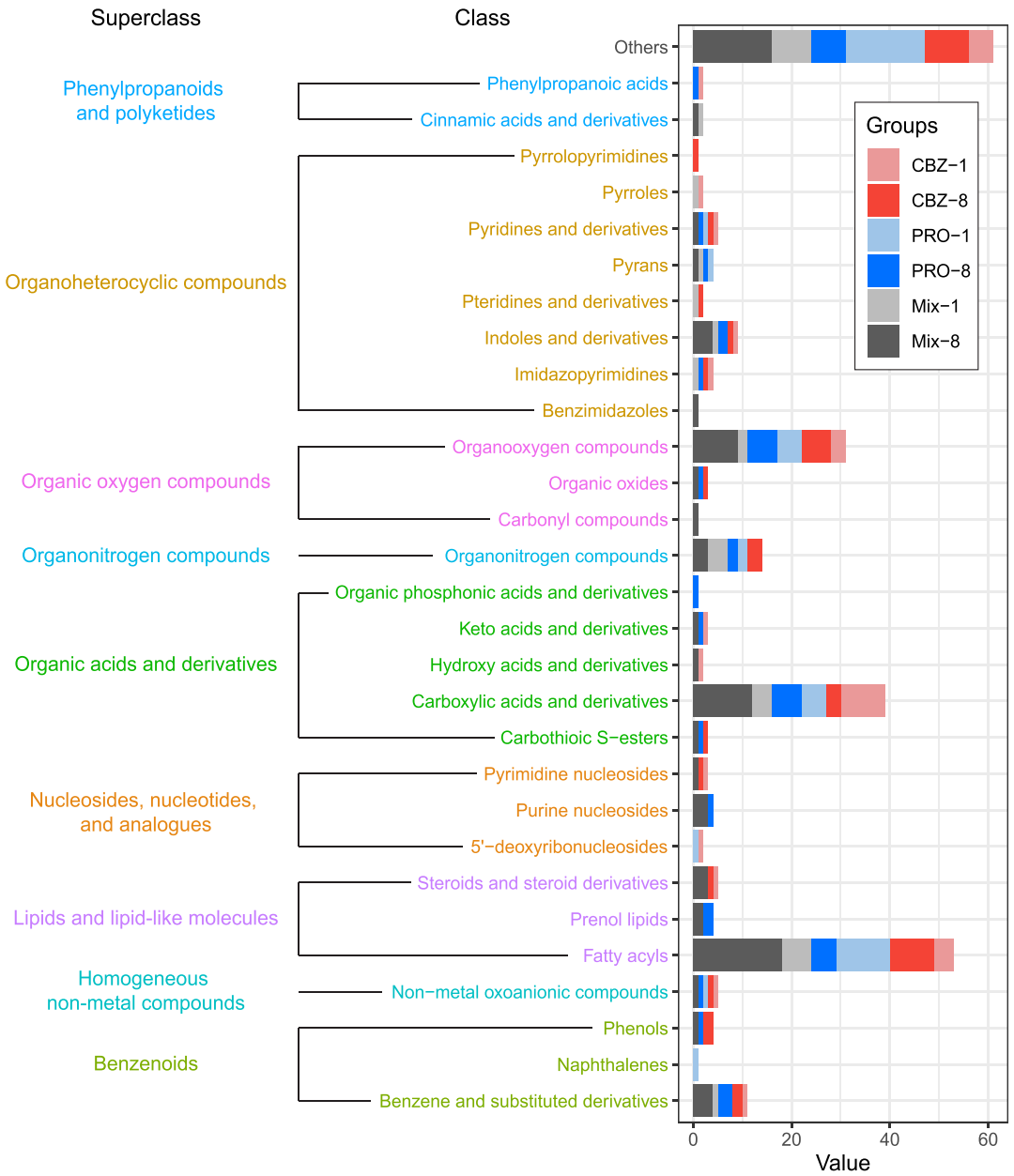


Figure 4. Superclass and class enrichment of hepatic differentially abundant metabolites The superclass and class enrichment of hepatic differentially abundant metabolites were done according to HMDB after 1 and 8 h of exposure to CBZ, PRO and Mix.

increasing and decreasing patterns after 1 and 8 h of exposure (Figure 7F).

The sPLS-DA results after CBZ, PRO and Mix exposure at 72 h

After 72 h of exposure, the sPLS-DA results showed that there was also a significant separation across the CBZ, PRO and Mix groups (Supplementary Figure S4A). In loadings 1 and 2, the differentially abundant metabolites with loading score > 0.5 were N-acetyl-D-galactosamine (M318T221) and D-iditol (M182T655) (Supplementary Figure S4B). The levels of N-acetyl-D-galactosamine were significantly increased in the Mix-72 h group compared with the CBZ-72 h and PRO-72 h groups (Supplementary Figure S4C). Additionally, the Mix-72 h group showed significantly lower levels of D-iditol than the individual CBZ and PRO groups (Supplementary Figure S4C).

Discussion

The excessive use of CBZ and PRO has led to the frequent detection of their residues in agricultural products and has attracted growing concern over recent decades. Some previous studies reported the individual toxic effects of CBZ and PRO on lipid metabolism [17,18], the inflammatory response [18], the gut microbiome [22], development [19] and reproduction in several different species. Zheng *et al.* [14] reported the coresidual nature of CBZ and PRO in the environment. However, the potential impact of combined CBZ and PRO exposure on public health remains unclear.

In this study, we conducted untargeted metabolomics analysis to

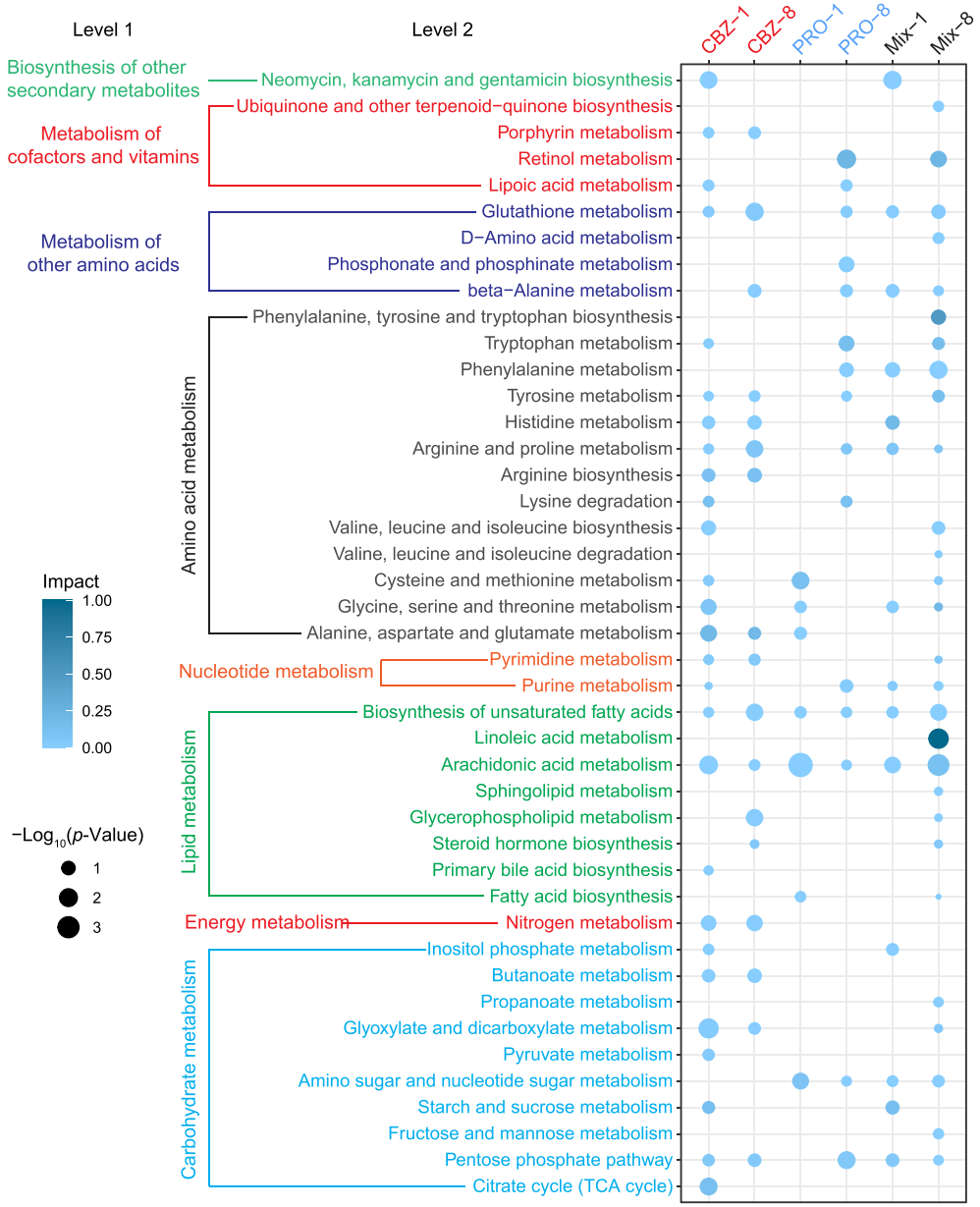


Figure 5. KEGG pathway enrichment analysis of hepatic differentially abundant metabolites KEGG pathway enrichment analysis of hepatic differentially abundant metabolites in the CBZ, PRO and Mix groups was performed at 1 and 8 h postexposure.

determine the combined toxic effects of CBZ and PRO in the liver after 1, 8 and 72 h of exposure. First, the sPLS-DA results showed that the three treatment groups had significant separations from the 0 h group (Figure 1B). After 1 and 8 h of exposure, the CBZ, PRO and Mix groups also had significant separation from the 0 h group (Figure 2A,D). Meanwhile, the Mix-8 h group was significantly separated from the individual treatment groups after 8 h of exposure (Figure 2D).

According to the HMDB, most differentially abundant metabolites were predominantly enriched in three classes: (1) fatty acyls, (2) carboxylic acids and derivatives and (3) organooxygen compounds (Figure 4). Our previous study demonstrated that individual CBZ (100 and 500 μg/L) exposure for 27 days in mice disrupted hepatic lipid metabolism, particularly by inducing hepatic lipid accumulation [22]. Among the fatty acyls class, we observed that the levels of 12-KETE were markedly increased after CBZ, PRO and Mix treatment (Supplementary Figure S3A). 12-KETE, a metabolite of 12-hydroperoxy-5,8,10,14-eicosatetraenoic acid (12-HPETE) [38], is an electrophilic oxo-lipid that selectively inhibits lipoxygenase activity [39] and activates human neutrophils [40]. In addition, Dozsa *et al.* [41] demonstrated that 12-KETE acts as an endogenous PPARγ ligand to regulate PPARγ signaling pathways. Our previous study demonstrated that individual exposure to CBZ and PRO induced hepatic *PPARγ* expression in mice and that combined exposure markedly enhanced *PPARγ* expression [42]. Furthermore, KEGG pathway enrichment results showed that the differentially abundant metabolites were enriched in several distinct pathways (Figure 5). For instance, some pathways were only enriched in CBZ-

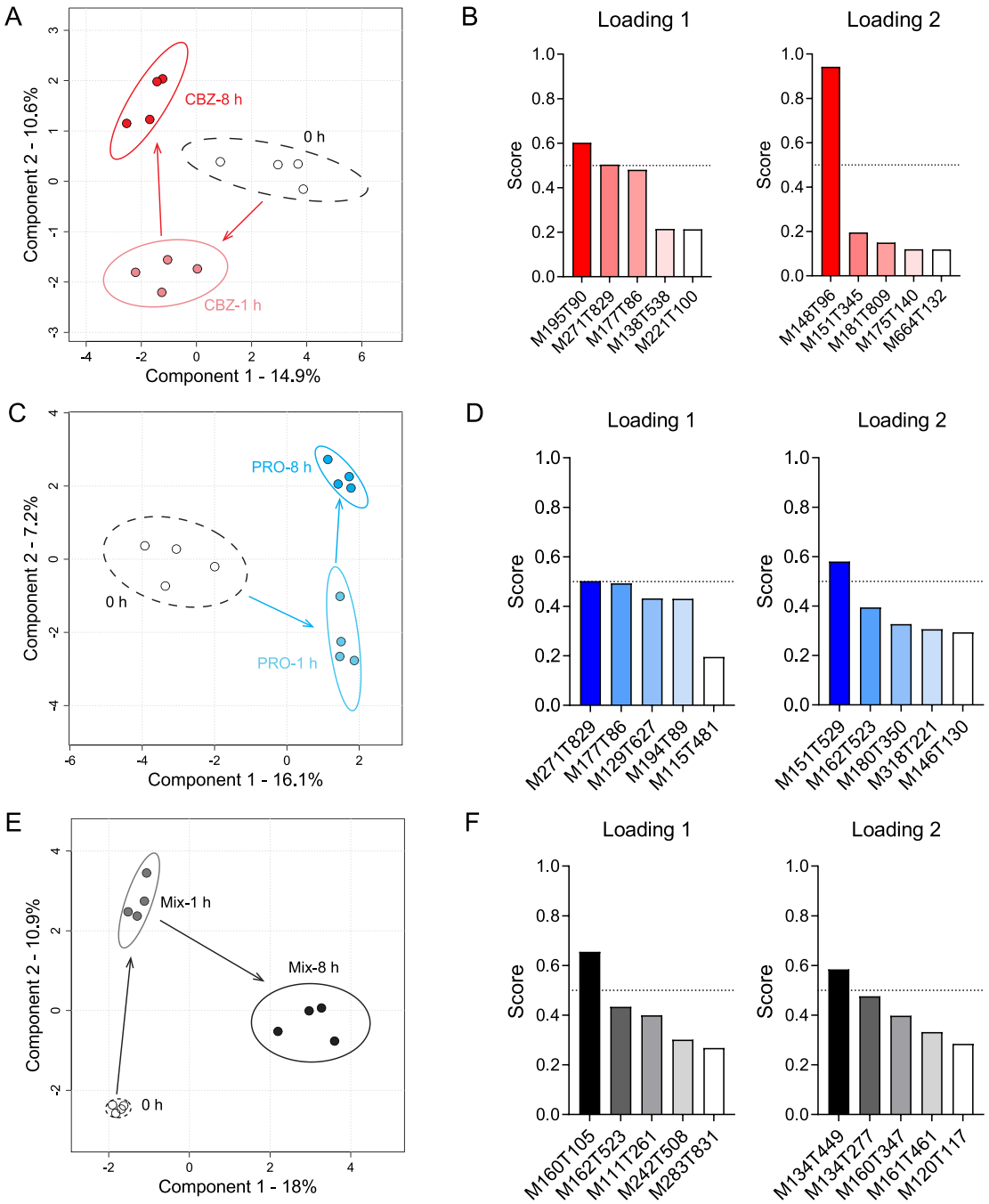


Figure 6. sPLS-DA results after CBZ, PRO and Mix exposure (A,C,E) The sPLS-DA results after exposure to (A) CBZ, (C) PRO and (E) Mix at 1 and 8 h. (B,D,F) The metabolites with the top 5 scores of loadings 1 and 2 in the (B) CBZ, (D) PRO and (F) Mix groups by sPLS-DA at 1 and 8 h postexposure.

treated groups, while others were unique to the PRO and Mix groups. Additionally, phenylalanine, tyrosine and tryptophan biosynthesis and linoleic acid metabolism with high impact were only enriched in the Mix-8 h group (Figure 5). The phenylalanine, tyrosine and tryptophan biosynthesis pathways were uniquely enriched in the Mix-8 h group, where L-tyrosine levels were significantly reduced (Figure 5 and Supplementary Figure S2D). Untargeted metabolomic results showed that individual PRO exposure affected abnormal hepatic amino acid levels in maternal mice and offspring [43]. For the linoleic acid metabolism pathway, the levels of linoleic acid and 13(S)-HPODE were significantly decreased in the Mix-8 h groups compared with those in the 0 h group (Supplementary Figure S2B). Some previous studies reported the alteration of linoleic acids after short- or long-term exposure to air pollution [44–46]. In addition, combined exposure to polystyrene microplastics and tetracycline induced a higher impact on linoleic acid metabolism pathway enrichment than individual exposure in *Oryzias melastigma* [47]. In adipose and liver, linoleic acid could evoke de-lipidation through the regulation of genes controlling lipid metabolism [48]. 13(S)-HPODE is produced by the

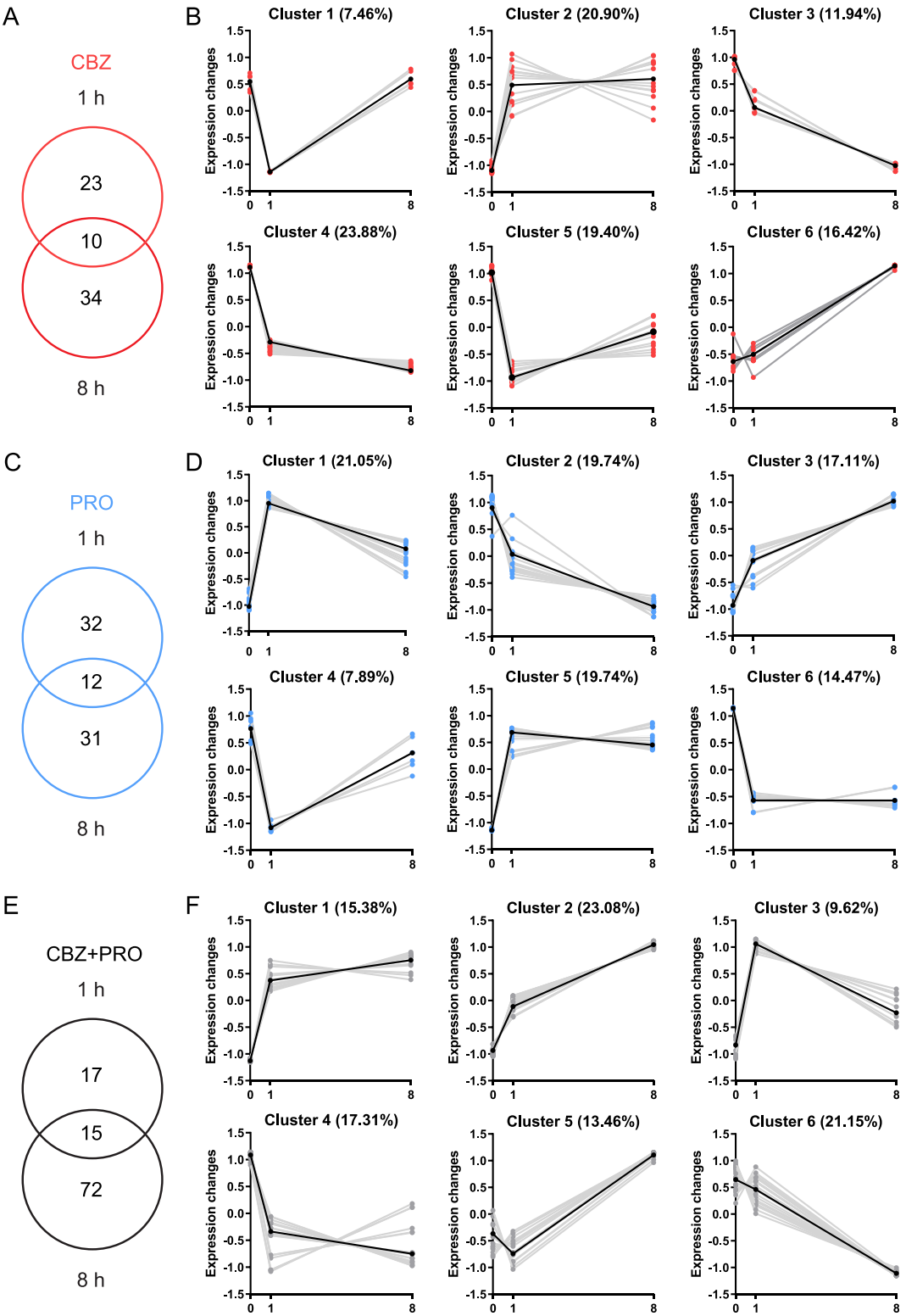


Figure 7. Time course of hepatic differentially abundant metabolites (A,C,E) Venn diagram of (A) CBZ, (C) PRO and (E) Mix groups between 1 and 8 h of exposure. (B,D,F) The time-course curves of (B) CBZ, (D) PRO and (F) Mix groups. Black lines indicate the average expression change of the differentially abundant metabolites in the cluster.

oxidation of linoleic acid by lipoxygenase [49]. Biosynthesis of unsaturated fatty acids and the arachidonic acid metabolism pathway were commonly enriched in the three treatment groups after 1 and 8 h of exposure (Figure 5A). Arachidonic acid metabolism is the pathway downstream of linoleic acid metabolism, and arachidonic acid and its keto-metabolites (*e.g.*, 12-KETE) may

act as endogenous ligands that activate PPARγ signaling [41,50]. Compared with individual exposure, combined exposure to CBZ and PRO produced a greater number of hepatic differentially abundant metabolites and revealed novel and mixture-specific toxic effects in the liver. Linoleic acid is a highly susceptible polyunsaturated fatty acid. Its dysregulation strongly suggests increased vulnerability to lipid peroxidation, which compromises oxidative stress and membrane integrity [51]. In addition, as a precursor to arachidonic acid, the alteration of linoleic acid metabolism and the arachidonic acid metabolism pathway suggested a disturbance in inflammatory regulation [52,53]. Some previous studies have also suggested that combined exposure to pesticides can enhance toxicity. For instance, Wang *et al.* [27] suggested that combined exposure to PRO and chlorothalonil in mice impaired the integrity of intestinal barrier function and caused glucolipid metabolism disorder in the liver. Moreover, combined exposure to fenvalerate and tebuconazole induced more severe inflammation and oxidative stress than individual exposure in the liver of Japanese medaka [54]. Similarly, co-exposure to polystyrene microplastics and cypermethrin disrupted gut microbial composition and enhanced antibiotic resistance gene complexity [55].

The sPLS-DA results revealed that the hepatic metabolite component changed over time after treatment (Figure 7). Most previous studies focused on a single timepoint after exposure and reported only whether metabolites significantly increased or decreased. A multiple timepoint transcriptomics study in the white shrimp *Litopenaeus vannamei* after nonylphenol exposure showed that differentially expressed genes clustered into 12 groups, such as continuously increasing, continuously decreasing, V shaped and inverted-V shaped patterns. [56]. In this study, distinct clusters of differentially abundant metabolites in the liver were also observed after 1 and 8 h of exposure (Figure 7). For the CBZ and Mix groups, most differentially abundant metabolites were clustered and showed continuously increasing and continuously decreasing patterns (Figure 7C,E). In the PRO groups, most differentially abundant metabolites showed inverted-V shaped and continuously decreasing patterns (Figure 7D). Time-course analysis indicated that hepatic differentially abundant metabolites after CBZ, PRO and Mix exposure had several patterns.

Although CBZ and PRO residues were generally undetectable in the liver at 72 h (unpublished data), these treatment groups showed distinct metabolic profiles (Supplementary Figure S4), implying persistent metabolic perturbations after short exposure. Overall, short-term combined exposure to CBZ and PRO induced synergistic metabolic disturbances in the liver. The Mix-8 h group exhibited the greatest number of differentially abundant metabolites, which were enriched primarily in fatty acyls and displayed unique high-impact enriched pathways in linoleic acid metabolism and phenylalanine, tyrosine and tryptophan biosynthesis. Time-course analysis showed diverse patterns of altered metabolites rather than a simple monotonic trend. These findings indicated that coexposure to CBZ and PRO might amplify hepatic metabolic disruption and highlighted the need to evaluate mixture exposures in human and ecological risk assessments.

Supplementary Data

Supplementary data are available at *Acta Biochimica et Biophysica Sinica* online.

Data Availability

Metabolomic analysis data are available at the National Genomics Data Center (No. OMIX014716). All other data can be accessed upon reasonable request from the corresponding authors.

Author Contributions

Zhiwei Bao: Conceptualization, Methodology and Writing – Original Draft; Ting Luo: Investigation and Visualization; Shiyi Hu: Investigation and Validation; Guiling Yang: Supervision, Writing – Review & Editing; Yuanxiang Jin: Supervision, Writing – Review & Editing, and Funding acquisition.

Funding

This work was supported by the grants from the National Natural Science Foundation of China (No. 42277279) and the Project funded by the China Postdoctoral Science Foundation (No. 2021M702903).

Conflict of Interest

The authors declare that they have no conflict of interest.

References

1. Ranjan B, Daundkar PS, Rampal S. Ameliorative effect of selenium on carbendazim induced oral sub-chronic testicular toxicity in bucks. *Small Ruminant Res* 2014, 119: 107–113
2. Davidse LC. Differential binding of methyl benzimidazol-2-yl carbamate to fungal tubulin as a mechanism of resistance to this antimitotic agent in mutant strains of *Aspergillus nidulans*. *J Cell Biol* 1977, 72: 174–193
3. Pappas AC, Fisher DJ. A comparison of the mechanisms of action of vinclozolin, procymidone, iprodione and prochloraz against *Botrytis cinerea*. *Pestic Sci* 1979, 10: 239–246
4. Magnucka EG, Suzuki Y, Pietr SJ, Kozubek A, Zarnowski R. Action of benzimidazole fungicides on resorcinolic lipid metabolism in rye seedlings depends on thermal and light growth conditions. *Pesticide Biochem Physiol* 2007, 88: 219–225
5. Xu X, Chen J, Li B, Tang L. Carbendazim residues in vegetables in China between 2014 and 2016 and a chronic carbendazim exposure risk assessment. *Food Control* 2018, 91: 20–25
6. Buch AC, Brown GG, Niva CC, Sautter KD, Sousa JP. Toxicity of three pesticides commonly used in Brazil to *Pontoscolex corethrurus* (Müller, 1857) and *Eisenia andrei* (Bouché, 1972). *Appl Soil Ecol* 2013, 69: 32–38
7. Li X, Zhou Q, Wei S, Ren W, Sun X. Adsorption and desorption of carbendazim and cadmium in typical soils in northeastern China as affected by temperature. *Geoderma* 2011, 160: 347–354
8. Barahona F, Gjelstad A, Pedersen-Bjergaard S, Rasmussen KE. Hollow fiber-liquid-phase microextraction of fungicides from orange juices. *J Chromatogr A* 2010, 1217: 1989–1994
9. Li Z, Nie J, Yan Z, Cheng Y, Lan F, Huang Y, Chen Q, *et al.* A monitoring survey and dietary risk assessment for pesticide residues on peaches in China. *Regulatory Toxicol Pharmacol* 2018, 97: 152–162
10. Abd-Elhaleem ZA. Pesticide residues in tomato and tomato products marketed in Majmaah province, KSA, and their impact on human health. *Environ Sci Pollut Res* 2020, 27: 8526–8534
11. Xiao J, Xu X, Wang F, Ma J, Liao M, Shi Y, Fang Q, *et al.* Analysis of exposure to pesticide residues from traditional Chinese medicine. *J Hazard Mater* 2019, 365: 857–867
12. Park DW, Kim KG, Choi EA, Kang GR, Kim TS, Yang YS, Moon SJ, *et al.* Pesticide residues in leafy vegetables, stalk and stem vegetables from South Korea: a long-term study on safety and health risk assessment. *Food*

Additives Contams-Part A 2016, 33: 105–118
13. Lin S, Tang T, Cang T, Yu S, Ying Z, Gu S, Zhang Q. The distributions of three fungicides in vegetables and their potential health risks in Zhejiang, China: a 3-year study (2015–2017). *Environ Pollut* 2020, 267: 115481
14. Zheng S, Chen B, Qiu X, Chen M, Ma Z, Yu X. Distribution and risk assessment of 82 pesticides in Jiulong River and estuary in South China. *Chemosphere* 2016, 144: 1177–1192
15. Readman JW, Albanis TA, Barcelo D, Galassi S, Tronczynski J, Gabrielides GP. Fungicide contamination of *Mediterranean estuarine* waters: results from a MED POL pilot survey. *Mar Pollution Bull* 1997, 34: 259–263
16. de Castro Lima JAM, Labanowski J, Bastos MC, Zanella R, Prestes OD, de Vargas JPR, Mondamert L, ***et al.*** "Modern agriculture" transfers many pesticides to watercourses: a case study of a representative rural catchment of southern Brazil. *Environ Sci Pollut Res* 2020, 27: 10581–10598
17. Bao Z, Zhao Y, Wu A, Lou Z, Lu H, Yu Q, Fu Z, ***et al.*** Sub-chronic carbendazim exposure induces hepatic glycolipid metabolism disorder accompanied by gut microbiota dysbiosis in adult zebrafish (*Daino rerio*). *Sci Total Environ* 2020, 739: 140081
18. Jin C, Zeng Z, Wang C, Luo T, Wang S, Zhou J, Ni Y, ***et al.*** Insights into a possible mechanism underlying the connection of carbendazim-induced lipid metabolism disorder and gut microbiota dysbiosis in mice. *Toxicol Sci* 2018, 166: 382–393
19. Farag A, Ebrahim H, ElMazoudy R, Kadous E. Developmental toxicity of fungicide carbendazim in female mice. *Birth Defects Res Pt B* 2011, 92: 122–130
20. Gray L. Carbendazim-induced alterations of reproductive development and function in the rat and hamster. *Fundamental Appl Toxicol* 1990, 15: 281–297
21. Nakai M, Miller MG, Carnes K, Hess RA. Stage-specific effects of the fungicide carbendazim on Sertoli cell microtubules in rat testis. *Tissue Cell* 2002, 34: 73–80
22. Jin Y, Zeng Z, Wu Y, Zhang S, Fu Z. Oral exposure of mice to carbendazim induces hepatic lipid metabolism disorder and gut microbiota dysbiosis. *Toxicol Sci* 2015, 147: 116–126
23. Ostby J, Kelce WR, Lambright C, Wolf CJ, Mann P, Gray Jr LE. The fungicide procymidone alters sexual differentiation in the male rat by acting as an androgen-receptor antagonist *in vivo* and *in vitro*. *Toxicol Ind Health* 1999, 15: 80–93
24. Wu A, Yu Q, Lu H, Lou Z, Zhao Y, Luo T, Fu Z, ***et al.*** Developmental toxicity of procymidone to larval zebrafish based on physiological and transcriptomic analysis. *Comp Biochem Physiol Part C-Toxicol Pharmacol* 2021, 248: 109081
25. Jardim ANO, Caldas ED. Pesticide residues in food of plant origin commercialized in Brazil from 2010 to 2020—an update from the two national monitoring programs. *Food Control* 2024, 165: 110674
26. Wade A, Lin CH, Kurkul C, Regan ER, Johnson RM. Combined toxicity of insecticides and fungicides applied to California almond orchards to honey bee larvae and adults. *Insects* 2019, 10: 20
27. Wang Y, Jin C, Wang D, Zhou J, Yang G, Shao K, Wang Q, ***et al.*** Effects of chlorothalonil, prochloraz and the combination on intestinal barrier function and glucolipid metabolism in the liver of mice. *J Hazard Mater* 2021, 410: 124639
28. Di S, Wang Y, Xu H, Wang X, Yang G, Chen C, Yang X, ***et al.*** Comparison the dissipation behaviors and exposure risk of carbendazim and procymidone in greenhouse strawberries under different application method: Individual and joint applications. *Food Chem* 2021, 354: 129502
29. Di S, Bao Z, Zhao H, Liu Z, Qi P, Wang Z, Jin Y, ***et al.*** Transcriptomic and metabolomic insights into the enantioselective effects of chiral fungicide penflufen and its enantiomers on multi-endpoints in the liver for mice. *J Hazard Mater* 2025, 496: 139419
30. Zhao Y, Qin Z, Huang Z, Bao Z, Luo T, Jin Y. Effects of polyethylene microplastics on the microbiome and metabolism in larval zebrafish. *Environ Pollut* 2021, 282: 117039
31. Yang G, Wang Y, Li J, Wang D, Bao Z, Wang Q, Jin Y. Health risks of chlorothalonil, carbendazim, prochloraz, their binary and ternary mixtures on embryonic and larval zebrafish based on metabolomics analysis. *J Hazard Mater* 2021, 404: 124240
32. Fang L, Fang C, Di S, Wang X, Jin Y. Rubber-derived contaminants N-(1,3-dimethylbutyl)-N′-phenyl-p-phenylenediamine and N-(1,3-dimethylbutyl)-N′-phenyl-p-phenylenediamine-quinone alter intergenerational cholesterol metabolism in F1 offspring of exposed mice. *Toxicol Lett* 2026, 416: 111826
33. Wang X, Hu L, Jin C, Qian M, Jin Y. Effects of maternal exposure to procymidone on hepatic metabolism in the offspring of mice. *Environ Toxicol* 2023, 38: 833–843
34. Pang Z, Chong J, Zhou G, de Lima Morais DA, Chang L, Barrette M, Gauthier C, ***et al.*** MetaboAnalyst 5.0: narrowing the gap between raw spectra and functional insights. *Nucleic Acids Res* 2021, 49: W388–W396
35. Wishart DS, Guo AC, Oler E, Wang F, Anjum A, Peters H, Dizon R, ***et al.*** HMDB 5.0: the human metabolome database for 2022. *Nucleic Acids Res* 2022, 50: D622–D631
36. Chen T, Zhang H, Liu Y, Liu YX, Huang L. EVenn: easy to create repeatable and editable Venn diagrams and Venn networks online. *J Genet Genomics* 2021, 48: 863–866
37. Kumar L, Futschik ME. Mfuzz: a software package for soft clustering of microarray data. *Bioinformation* 2007, 2: 5–7
38. Piomelli D, Feinmark SJ, Shapiro E, Schwartz JH. 12-Keto-eicosatetraenoic acid a biologically active eicosanoid in the nervous system of aplysia. *Ann New York Acad Sci* 1989, 559: 208–218
39. Armstrong MM, Diaz G, Kenyon V, Holman TR. Inhibitory and mechanistic investigations of oxo-lipids with human lipoxygenase isozymes. *Bioorg Med Chem* 2014, 22: 4293–4297
40. Naccache PH, Leblanc Y, Rokach J, Patrignani P, Laclos BF, Borgeat P. Calcium mobilization and right-angle light scatter responses to 12-oxo-derivatives of arachidonic acid in neutrophils: evidence for the involvement of the leukotriene B4 receptor. *Biochim Biophys Acta* 1991, 1133: 102–106
41. Dozsa A, Dezso B, Toth BI, Bacsi A, Poliska S, Camera E, Picardo M, ***et al.*** PPARγ-mediated and arachidonic acid-dependent signaling is involved in differentiation and lipid production of human sebocytes. *J Investig Dermatol* 2014, 134: 910–920
42. Bao Z, Wang D, Zhao Y, Luo T, Yang G, Jin Y. Insights into enhanced toxic effects by the binary mixture of carbendazim and procymidone on hepatic lipid metabolism in mice. *Sci Total Environ* 2023, 882: 163648
43. Wang X, Weng Y, Geng S, Wang C, Jin C, Shi L, Jin Y. Maternal procymidone exposure has lasting effects on murine gut-liver axis and glucolipid metabolism in offspring. *Food Chem Toxicol* 2023, 174: 113657
44. Liang D, Moutinho JL, Golan R, Yu T, Ladva CN, Niedzwiecki M, Walker DI, ***et al.*** Use of high-resolution metabolomics for the identification of metabolic signals associated with traffic-related air pollution. *Environ Int* 2018, 120: 145–154
45. Zhu K, Browne RW, Blair RH, Bonner MR, Tian M, Niu Z, Deng F, ***et al.*** Changes in arachidonic acid (AA)- and linoleic acid (LA)-derived hydroxy metabolites and their interplay with inflammatory biomarkers in response

to drastic changes in air pollution exposure. *Environ Res* 2021, 200: 111401

46. Yan Z, Li S, Chen R, Xie H, Wu M, Nan N, Xing Q, ***et al.*** Effects of differential regional $PM_{2.5}$ induced hepatic steatosis and underlying mechanism. *Environ Pollut* 2023, 323: 121220
47. Zhao P, Lu W, Avellán-Llaguno RD, Liao X, Ye G, Pan Z, Hu A, ***et al.*** Gut microbiota related response of *Oryzias melastigma* to combined exposure of polystyrene microplastics and tetracycline. *Sci Total Environ* 2023, 905: 167359
48. House RL, Cassady JP, Eisen EJ, McIntosh MK, Odle J. Conjugated linoleic acid evokes de-lipidation through the regulation of genes controlling lipid metabolism in adipose and liver tissue. *Obes Rev* 2005, 6: 247–258
49. Hershelman D, Kahler KM, Price MJ, Lu I, Fu Y, Plumeri PA, Karaisz F, ***et al.*** Oxygenation reactions catalyzed by the F557V mutant of soybean lipoxygenase-1: evidence for two orientations of substrate binding. *Arch Biochem Biophys* 2019, 674: 108082
50. Hanna VS, Hafez EAA. Synopsis of arachidonic acid metabolism: a review. *J Adv Res* 2018, 11: 23–32
51. Ayala A, Muñoz MF, Argüelles S. Lipid peroxidation: production, metabolism, and signaling mechanisms of malondialdehyde and 4-hydroxy-2-nonenal. *Oxid Med Cell Longev* 2014, 2014: 1–31
52. Wang T, Fu X, Chen Q, Patra JK, Wang D, Wang Z, Gai Z. Arachidonic acid metabolism and kidney inflammation. *Int J Mol Sci* 2019, 20: 3683
53. Ma Y, Jiang J, Zhao C, Wei B, Gao J. Arachidonic acid metabolism in metabolic dysfunction-associated steatotic liver disease and liver fibrosis. *Hepatol Commun* 2025, 9: e0802
54. Jawad M, Xu H, Nasir S, Yin J, Wu C, Wang A, Hong N, ***et al.*** Microbial dysbiosis and hepatic inflammation under combined pesticide exposure: insights into gut-liver axis disruption in Japanese medaka. *J Hazard Mater* 2025, 499: 140295
55. Fang C, Zhu J, Xu H, Qian M, Jin Y. Polystyrene microplastics and cypermethrin exposure interfered the complexity of antibiotic resistance genes and induced metabolic dysfunction in the gut of adult zebrafish. *Environ Pollut* 2025, 374: 126288
56. Guo H, Liang Z, Zheng P, Li L, Xian J, Zhu X. Effects of nonylphenol exposure on histological changes, apoptosis and time-course transcriptome in gills of white shrimp *Litopenaeus vannamei*. *Sci Total Environ* 2021, 781: 146731